

Laser Guide Star for 3.6m and 8m telescopes: Performances and astrophysical implications

M. Le Louarn^{1, 2}, R. Foy², N. Hubin¹ and M. Tallon²

¹*ESO - European Southern Observatory, Karl-Schwarzschild-Straße 2, Garching bei München, D-85748 Federal Republic of Germany*

²*CRAL - Centre de Recherche astronomique de Lyon, 9 av. Charles André, F-69561 Saint Genis Laval, France*

E-mail: lelouarn@eso.org, nhubin@eso.org, foy@obs.univ-lyon1.fr, mtallon@obs.univ-lyon1.fr

Received ???, 1997; accepted ??, ??

ABSTRACT

We have constructed an analytical model to simulate the behavior of an adaptive optics system coupled with a sodium laser guide star. The code is applied to a 3.6-m and 8m class telescopes. The results are given in terms of Strehl ratio and full width at half maximum of the point spread function. Two atmospheric models are used, one representing good atmospheric conditions (20 per cent of the time), the other median conditions.

Sky coverage is computed for natural guide star and laser guide star systems, with two different methods. The first one is a statistical approach, using stellar densities, to compute the probability to find a nearby reference. The second is a cross-correlation of a science object catalogue and the USNO catalogue. Results are given in terms of percentage of the sky that can be accessed with given performances, and in terms of number of science object that can be observed, with Strehls greater than 0.2 and 0.1 in K and J bands.

Key words: atmospheric effects – telescopes

1 INTRODUCTION

The angular resolution of ground based telescopes has been limited for a long time by the atmospheric turbulence. The resolution was typically that of a telescope 10 - 20 cm in aperture. The concept of adaptive optics (AO) was first proposed by Babcock (1953). This technique allows to correct, in real time, the atmospheric turbulence. It provides nearly diffraction limited images in the near infrared domain.

For the AO system to function, a reference source must be found close to the astronomical object. It must provide sufficient signal to noise ratio to the wave-front sensor (WFS) so that the wavefront can be measured accurately. Several other solutions can be used to provide this reference. The first one is to use the science object itself, provided it is bright enough. The second solution is to use a nearby star. It has to be bright enough, but it must also be close to the science object, within the isoplanatic patch. The two previous solutions are called Natural Guide Star (NGS) AO systems. A third solution, proposed by Foy & Labeyrie (1985) is to use a laser beam to create an artificial laser guide star (LGS).

Two types of laser stars can be used, following two principles: Rayleigh and Mie scattering in the first 10 to 20 km of the atmosphere (see e.g. (Fugate et al. 1994), (Laurent

et al. 1995)) or resonant scattering by sodium atoms near 90 km (see e.g. (Max et al. 1994)).

There are two main problems with the LGS. First, the image motion created by atmospheric turbulence (tip-tilt) can not be sensed with the LGS, due to the round trip of light. Rigaut & Gendron (1992), showed that this is a severe limitation of the LGS, preventing full sky coverage, and proposed the concept of dual adaptive optics to increase the coverage by correcting the tilt-reference star itself with a second AO system, to increase the signal to noise ratio of the tilt measurement. Other solutions have been proposed: one can take short exposure images, to freeze the image motion. These short exposure images are diffraction limited (because of the LGS correction) and speckle-type algorithms can then be used. The gain compared to conventional speckle imaging is a gain in S/N ratio, due to the AO correction (see Tessier (1997) for an analysis of the gain brought by short exposure imaging in AO). The concept of the polychromatic artificial star (Foy et al. 1995), in which the tilt information is retrieved from laser spots produced at different wavelengths, gives promising results (Friedman et al. 1996) and could solve this problem. Another alternative would be a combination of different methods relying on the observation of the laser spot against the sky background (Ragazzoni (1997)).

The second limitation of the LGS is the cone effect (also called focus anisoplanatism). Since the laser star is at a fi-

arXiv:astro-ph/9710130v1 13 Oct 1997

nite distance from the telescope, compared to the science object, the light coming from the laser star does not probe exactly the same volume of turbulence than the light coming from the science object. This leads to a mis-measurement of the wavefront, and loss of correction quality. The cone effect is reduced if the artificial star is located high in the atmosphere. Therefore, sodium laser guide stars seem to be better suited for astronomical applications. Approaches using multiple guide stars have been proposed to counter this effect which is severe on the new 8 to 10 meter class telescopes (e.g. Tallon & Foy (1990), Jankevics & Wirth (1991), Johnston & Welsh (1994)).

With NGS-AO systems, the sky coverage is limited to the areas where reference stars can be found. Typically, the sky coverage is only a few percents, in the most optimistic cases. Because of the tilt determination problem, the sky coverage of LGS systems must also be computed. The goal of this study is to compute the sky coverage for two different systems equipped with sodium laser guide stars. The first is a 3.6m telescope, representing the current generation of instruments, for which a laser guide star upgrade is considered. The second system is an 8m class telescope, representing the new generation, for which we want to know if a LGS can significantly improve the performances. The 3.6m class telescope study is representative of an upgraded version of the ADONIS (Adaptive Optics Near Infra-red System) system (Beuzit et al. 1994) located in La Silla (Chile). The 8m class case can be seen as a model of the VLT (Very Large Telescope), which is under construction in Cerro Paranal, also in Chile. This telescope will be equipped with the NAOS (Nasmyth Adaptive Optics System) system, working in the near infrared. The results can be used however for other systems, since the atmospheric models can be representative of a good astronomical site. In the next section, we describe the models used to simulate the AO system and the laser star coupled with it. In section 3, we estimate the performances of these two systems in terms of achievable Strehl ratio and Full Width at Half Maximum (FWHM) of the PSF. The sky coverage is computed, with two different approaches. The first one uses stellar densities found with synthetic models of our Galaxy. The second is to make cross correlations of catalogues containing science targets and a catalogue containing reference stars. This ‘‘observer’s approach’’ can give lower limits on the number of objects that can really be observed, and in which conditions. In section 4, we study the performances that can be expected of an 8m telescope in the red part of the spectrum. In section 5, we present our conclusions.

2 LASER GUIDE STAR / AO SIMULATION

2.1 Atmospheric model

For a simulation of an AO system parameters describing the atmosphere must be defined. The seeing describes the effect that turbulence has on the long exposure image. It is expressed in arc-seconds and represents the FWHM of the image, as viewed through an un-compensated imager:

$$FWHM_s \approx \frac{\lambda}{r_0} \quad (1)$$

where λ is the considered wavelength and r_0 is Fried’s coherence length (Fried (1966)), at that wavelength:

$$r_0 = (0.423k^2 \sec(\zeta)\mu_0)^{-\frac{3}{5}} \quad (2)$$

where k is the wavenumber, ζ the zenith angle, and μ_n is the n^{th} moment of turbulence:

$$\mu_n = \int dh C_n^2(h) h^n \quad (3)$$

$C_n^2(h)$ is the refractive index fluctuation structure coefficient, and h is the height in the atmosphere.

Histograms of the seeing in La Silla and Paranal are shown on Fig 1. These histograms are obtained at the two sites for several years. Therefore, seasonal variations are smoothed out.

Measurement of $C_n^2(h)$ profiles made by SCIDAR or balloon (Sarazin (1990), Fuchs & Vernin (1993)) show that turbulence is usually concentrated in a few thin layers. Therefore, we have chose to use the approximation of infinitely thin turbulent layers. We used three layers to model the $C_n^2(h)$ profile. One represents the seeing close to the ground (telescope - mirror - dome), and two layers of atmospheric turbulence. The height of these layers were chosen so as to match the measured profiles.

Two atmosphere models were considered for each site, in order to study what effects variability in the $C_n^2(h)$ profile would have on the results. Therefore, we considered a good atmospheric condition case (obtained 20 per cent of the time), along with a median case (50 per cent of the time). These models are good and median in two ways: the better case represents good seeing condition, with a favorable turbulence profile (large isoplanatic angle). The median model is more pessimistic both in terms of seeing and isoplanatic angle. Therefore, with these models, it should be possible to span all the possible conditions that will be encountered.

Wind profiles are necessary to assess the temporal behavior of the atmosphere. For the Paranal wind profile, a modified Bufton wind profile was used (Bonaccini (1996)). For La Silla, we used a similar model but the low altitude wind-layer was modified according to balloon measurements made during the LASSCA campaign.

$$v(h) = a_1 + a_2 \cdot e^{-\left(\frac{h-10000}{h_2}\right)^2} + a_3 \cdot e^{-\left(\frac{h-5000}{h_3}\right)^2} \quad (4)$$

$v(h)$ is in meters per second and h in meters above the observatory. We used: $a_1 = 5$, $a_2 = 25$, $a_3 = 10$, $h_2 = 2000$, $h_3 = 500$. For Paranal: $a_1 = 5$, $a_2 = 25$, $a_3 = 18$, $h_2 = 2000$, $h_3 = 500$. Table 1 summarizes the atmospheric parameters.

In this table: $h_{ao} = (\mu_{5/3}/\mu_0)^{3/5}$ is the weighted altitude of turbulence for Adaptive Optics (Roddier, Gilli & Vernin 1982), and $\theta_0 = (2.91k^2 \sec(\zeta)^{8/3} \mu_{5/3})^{-3/5}$ is the isoplanatic angle (in arc-seconds) (Fried (1982)), and τ_0 is the correlation time of the atmosphere (Greenwood (1977)):

$$\tau_0 = (2.91k^2 \sec(\zeta)v_{5/3})^{-3/5} \quad (5)$$

where $v_n = \int dh C_n^2(h)v(h)^n$ is the n^{th} wind moment.

2.2 The NGS AO simulation

In the following section, we concentrate on the NGS-AO performances for the 3.6m and 8m telescopes. This simulation is based on analytical or semi analytical formulae.

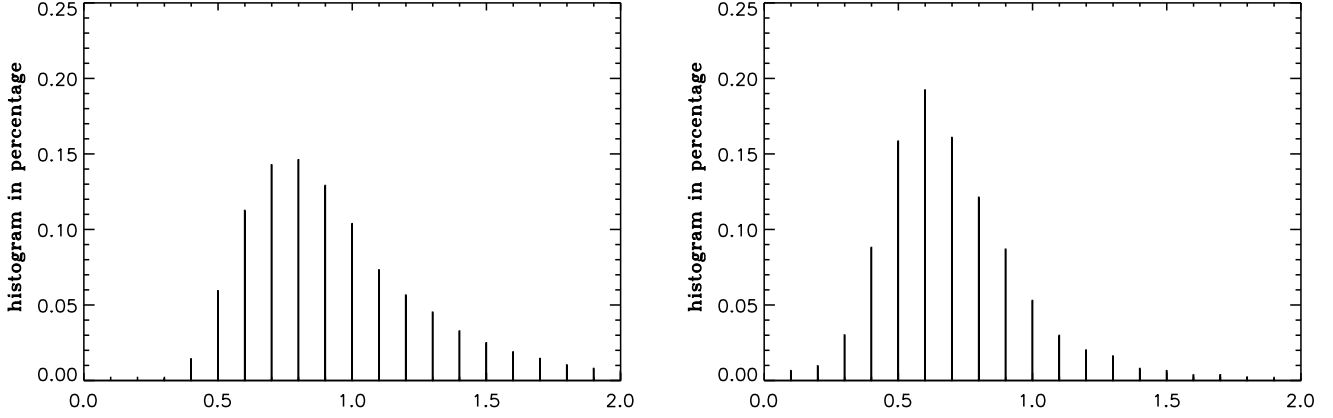


Figure 1. Histogram of seeing (in arcsec) at La Silla (left), Paranal (right)

Table 1. Atmospheric parameters

	La Silla (good)	La Silla (med.)	Paranal (excel.)	Paranal (good)	Paranal (med.)
Seeing ¹ (")	0.6	0.9	0.3	0.5	0.7
Dome seeing(")	0.8	0.8	0.0	0.0	0.0
% 1 st layer ²	0.8	0.5	0.9	0.89	0.7
% 2 nd layer ²	0.2	0.5	0.1	0.11	0.3
H_1 (km)	1.5	3.0	2.5	2.5	2.5
H_2 (km)	12.0	12.0	10.0	10.0	10.0
θ_0^1 (")	2.3	0.9	6.0	3.5	1.7
h_{ao} (km)	2.7	5.8	3.6	3.8	5.5
τ_0^1 (ms)	5.0	3.1	11.4	6.6	3.0

¹: at 0.5 μm , zenith

²: in % of the total atmospheric seeing

The AO system simulation is made of two main parts: the tip-tilt correction loop and the higher order correction path.

Tip-tilt sensing is performed with quad-cell avalanche photodiodes (APDs). We considered three error sources: delay error, photon noise and sensor noise. We took a small (0.1 electrons rms) additive noise on the APDs to allow for some imperfection.

The delay error is caused by the lag between the sensor measurement and the applied correction. We supposed that the lag is only due to the integration time on the sensor. We compared several expressions for $\sigma_{\text{del}_t}^2$, the variance caused by the delay (Olivier & Gavel (1994), (Sandler et al. 1994), Parenti & Sasiela (1994)). The results were very similar. We chose the last reference, giving the most pessimistic result:

$$\sigma_{\text{del}_t}^2 = 4.09 \cdot \sec(\zeta) D^{-7/3} v_{-1/3}^{8/15} v_{14/3}^{7/15} \tau_{\text{dt}}^2 \quad (6)$$

where τ_{dt} is the tilt correction delay and D the telescope diameter.

Photon noise arises from the quantum nature of light. It was also taken from Parenti & Sasiela (1994), which gives

similar results as Rousset (1994). Its variance, $\sigma_{\text{ph}_t}^2$, was computed according to:

$$\sigma_{\text{ph}_t}^2 = \frac{4}{3} \pi^2 \left(\frac{k_t}{k_{sc}} \right)^{12/5} \frac{1}{N_{\text{ph}_t}} \quad (7)$$

where k_t and k_{sc} are the wavenumbers of the tilt sensor and science camera, respectively, T_{tilt} is the transmission of the tilt path and η_{tilt} is the quantum efficiency of the tilt sensor, N_{ph_t} is the number of photons per sub-aperture and exposure time:

$$N_{\text{ph}_t} = \frac{\pi^2}{2hc k_t} T_{\text{tilt}} \eta_{\text{tilt}} \tau_{\text{dt}} D^2 I_t \quad (8)$$

where I_t is the irradiance (in W/m^2) at the tilt sensor.

σ_{nt}^2 , the wavefront variance caused by sensor additive noise is from Rousset (1994) which seems to fit better the low fluxes reference stars than Parenti & Sasiela (1994). It was slightly modified, using the method described in Parenti & Sasiela (1994) to take into account closed-loop operation, contributing a factor 2/3 to the variance:

$$\sigma_{\text{nt}}^2 = \frac{128}{9} \pi^2 \frac{1}{k_t^2} \frac{N_{\text{rms}}^2}{D^2 N_{\text{ph}_t}^2} \left(\frac{k_t}{k_{sc}} \right)^{12/5} \left(\frac{D}{r_0} \right)^2 \quad (9)$$

where N_{rms} is the rms readout noise of the detector.

To get the total noise, we assumed uncorrelated errors:

$$\sigma_{\text{tilt}}^2 = \sigma_{\text{del}_t}^2 + \sigma_{\text{ph}_t}^2 + \sigma_{\text{nt}}^2 \quad (10)$$

The WFS was modeled in a similar way. We used a system based on a Shack-Hartmann (SH) wave front sensor and a CCD. The error sources that appear with the WFS will now be described.

The fitting error depends only of the deformable mirror (DM). It appears because the actuator spacing is not infinitely small, so all spatial frequency aberrations cannot be compensated. We used Greenwood (1979) for σ_{fit}^2 , the fitting error variance:

$$\sigma_{\text{fit}}^2 = 0.34 \cdot \left(\frac{d_s}{r_0} \right)^{\frac{5}{3}} \quad (11)$$

where d_s is the size of a square sub-pupil.

Another source of error associated with the DM and the WFS is the aliasing error. It results from the spectral

aliasing of the high order modes into lower order modes. Therefore, the measurement of the wavefront is biased. The expression for this variance, σ_{alias}^2 , is from Rigaut (1996):

$$\sigma_{\text{alias}}^2 = 0.2 \cdot \left(\frac{d_s}{r_0}\right)^{\frac{5}{3}} \quad (12)$$

The sum of the aliasing and fitting error variances fixes the maximum Strehl that can be achieved with an AO system. We have:

$$\sigma_{\text{alias}}^2 + \sigma_{\text{fit}}^2 = 0.54 \cdot \left(\frac{d_s}{r_0}\right)^{\frac{5}{3}} \quad (13)$$

This is in agreement with the 0.5 coefficient proposed by Parenti & Sasiela (1994) and 0.54 (Sandler et al. 1994).

There are also sources of error similar to those of the tilt sensor. Like for tilt, sensor noise σ_n^2 was derived from Rousset (1994):

$$\sigma_n^2 = \frac{8}{9} \pi^2 \left(\frac{k_{\text{sc}}}{k_{\text{wfs}}}\right)^2 \frac{N_{\text{rms}}^2 N_{\text{cen}}^4}{N_{\text{ph}}^2} \left(1 + \left(\frac{k_{\text{wfs}}}{k_{\text{sc}}}\right)^{12/5} \left(\frac{d_s}{r_0}\right)^2\right) \left(\frac{k_{\text{sc}}}{k_{\text{wfs}}}\right)^{12/5} \left(\frac{r_0}{d_s}\right)^2 \quad (14)$$

where k_{wfs} is the wavenumber of the wavefront-sensor, η_{wfs} its quantum efficiency and T_{wfs} the transmission of the WFS path. τ_d is the integration time of the WFS and N_{ph} is the number of photons per sub-pupil per integration time:

$$N_{\text{ph}} = \frac{2\pi}{hck_{\text{wfs}}} T_{\text{wfs}} \eta_{\text{wfs}} \tau_d d_s^2 I_{\text{wfs}} \quad (15)$$

where I_{wfs} is the irradiance (in W/m²) at the WFS.

We used the photon noise expression given by Parenti & Sasiela (1994):

$$\sigma_{\text{ph}}^2 = \frac{4\pi^2}{3} \left(\frac{k_{\text{sc}}}{k_{\text{wfs}}}\right)^2 \frac{1}{N_{\text{ph}}} \quad (16)$$

The bandwidth error (or time delay error) σ_{del}^2 is the same effect than with tip-tilt time delay, but applied to the high order modes. We considered:

$$\sigma_{\text{del}}^2 = 0.962 \left(\frac{\tau_d}{\tau_0}\right)^{\frac{5}{3}} \quad (17)$$

The different error sources were assumed to be uncorrelated:

$$\sigma_{\text{ho}}^2 = \sigma_{\text{alias}}^2 + \sigma_{\text{fit}}^2 + \sigma_{\text{del}}^2 + \sigma_{\text{ph}}^2 + \sigma_n^2 \quad (18)$$

The noise of the sky background was taken into account by replacing N_{rms} with an equivalent noise N_{eq} according to:

$$N_{\text{eq}} = \sqrt{N_{\text{rms}}^2 + N_{\text{sky}}} \quad (19)$$

where N_{sky} is the number of electrons of noise coming from the sky background (set to $m_{\text{R}} = 21.5$). It is small in the red, where the wavefront sensing is done. However, it becomes non-negligible in the LGS case with tilt sensing on a natural guide star. The sky-background was assumed to be recorded before the loop is closed and therefore only the sky background remains. We converted magnitudes to fluxes with:

$$I = 10^4 \cdot \Delta\lambda \cdot 10^{-\left(\frac{m}{2.5} - ZP\right)} \quad (20)$$

where I is the irradiance (in W/m²), m is the magnitude, $\Delta\lambda$ is the bandwidth (in microns), and ZP the magnitude

Table 2. Simulation parameters

	3.6-m	8m
D (m)	3.6	8.0
d_s (m) (minimum)	0.5	0.5
η (WFS-Tilt)	0.9 - 0.6	0.9 - 0.6
$\Delta\lambda$ (WFS-Tilt) (μm)	0.3 - 0.4	0.3 - 0.4
$T_{\text{wfs}} - T_{\text{tilt}}$	0.35 - 0.30	0.40 - 0.35
N_{rms} (WFS-Tilt)	4.0 - 0.1	3.0 - 0.1

zero point (-11.75 in R). Table 2 sums up the instrumental parameters used in this study.

Computing the long exposure Strehl ratio, S_{le} , from the wavefront variance is a non-trivial matter, when these variances are high (typically more than $3 - 4\text{rad}^2$). Parenti (1992) assumes that the PSF consists of two components: a diffraction limited core and a halo. The width of the halo is that of an uncompensated image. In reality, this halo is narrower than the seeing disk (e.g. (Rigaut et al. 1997b)), but this approximation is good enough for our purpose. It is more accurate at high wavefront variances than identifying the Strehl with the coherent energy ($S = e^{-\sigma^2}$).

The FWHM of the PSF can also be estimated, using the same reference:

$$S_{\text{le}} = \frac{e^{-\sigma_{\text{ho}}^2}}{1 + \frac{\pi^2}{2} \left(\frac{D}{\lambda_{\text{sc}}}\right)^2 \sigma_{\text{tilt}}^2} + \frac{1 - e^{-\sigma_{\text{ho}}^2}}{1 + \left(\frac{D}{r_0}\right)^2} \quad (21)$$

$$FWHM = 1.03 \frac{\lambda_{\text{sc}}}{D} \frac{\left\{ \frac{e^{-2\sigma_{\text{ho}}^2}}{\left[1 + \frac{\pi^2}{2} \left(\frac{D}{\lambda_{\text{sc}}}\right)^2 \sigma_{\text{tilt}}^2\right]} + \frac{(1 - e^{-\sigma_{\text{fig}}^2})^2}{\left(1 + \frac{D}{r_0}\right)^2} \right\}^{1/2}}{S_{\text{le}}} \quad (22)$$

where σ_{ho} is the figure error, σ_{tilt} is the tilt error and λ_{sc} the science wavelength.

To get τ_{dt} and τ_d , the integration times on the tip-tilt and wavefront sensors, we used a Powell optimization algorithm to find the integration times that yield maximum Strehl. The maximum sampling frequency is set by the AO system hardware and therefore was limited to 500 Hz.

Another optimization scheme was to change the size of the sub-pupils (from 0.5 m, 1.0 m, 2.0 m corresponding on the 8m telescope to 16x16, 8x8, 4x4 SH configurations). This method was applied for all NGS results presented in this article. It allows to increase by approximately 1 the limiting magnitude in the 8m case. For LGS results, it was checked that the optimum configuration was the one with the smallest possible sub-apertures.

Another source of error is introduced if an off-axis reference source is used, instead of the science object. The method to compute σ_{aniso}^2 , the variance caused by anisoplanatism is described in Chassat (1989):

$$\sigma_{\text{aniso}}^2(\alpha) = 2(C_{nn}(0) - C_{nn}(\alpha)) \quad (23)$$

$$C_{nn}(\alpha) = \left(\frac{D}{r_0}\right)^{\frac{5}{3}} \frac{\int dh C_n^2(h) S_n\left(\frac{\alpha h}{D/2}\right)}{\int dh C_n^2(h)} \quad (24)$$

$$S_n(x) = 3.90(n+1) \int_0^\infty dk k^{-14/3} J_{n+1}^2(k) J_0(xk) \quad (25)$$

where α is the angle between the reference and the science object, n is the radial degree of the considered modes, $J_m(x)$

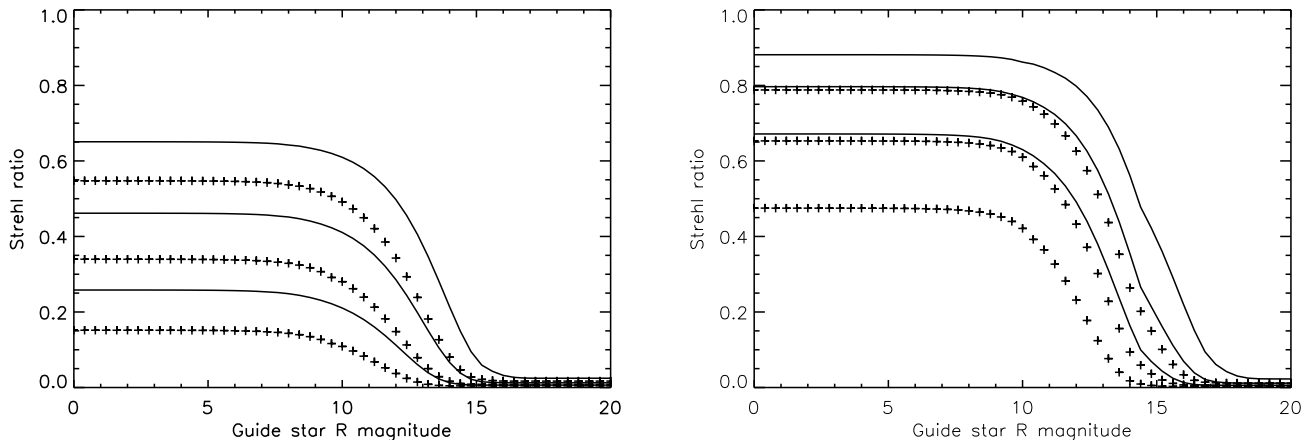


Figure 2. Predicted Strehl vs guide star magnitude for 3.6m (left) and 8m(right), at $2.2 \mu\text{m}$, $1.65 \mu\text{m}$, $1.25 \mu\text{m}$, good model (solid) and median model(crosses).

is the Bessel function of order m . The variances for anisoplanatism are then added in eq. 10 ($n = 1$) and eq. 18 ($n = 2$ to 10).

The results are in Fig 3. At $2.2 \mu\text{m}$, for a good atmospheric model, a Strehl attenuation of 50 per cent occurs at 30 arcsec. This is a fairly fast drop, since 80 per-cent of the Strehl is lost at 45 arc-seconds, for the same conditions.

The Strehl versus magnitude of guide star magnitude is plotted in Fig 2. For the 3.6-m case, peak performance is achieved down to a guide star magnitude of 10. At m_R 14, the Strehl is 0.2 in K, for the good atmospheric model. It drops to 0.1 with the median model. For the 8m case, peak performance ($S=0.86$) is also achieved to $m_R = 10$. $S=0.2$ is reached at magnitude 16, for the good model, in K. The improvement in performances between the two systems, which have the same sub-aperture size, is mainly due to a better seeing, and in lesser extent to better hardware characteristics (e.g. less readout noise in the CCD). Static aberrations, which can reduce significantly the Strehl ratio have not been taken into account in this study. Therefore, in a real system, the peak Strehl ratio at $2.2 \mu\text{m}$ should be reduced by about 10 per cent with a careful design.

2.3 AO simulation validation

The validity of this analytic model was checked with a full numerical simulation of the AO system. This code, developed by F. Rigaut (Rigaut et al. 1997a) uses Kolmogorov phase screens, simulates SH images, calculates the centroids and deduces the DM commands. The outputs are short and long exposure PSFs.

We simulated the 8m AO system with this code. Integration time, thresholds, sub-aperture configuration, loop gain were optimized to get the best Strehl ratio. Fig 4 shows that there is good agreement between analytical and numerical models. However the analytical model gives systematically better results than the numerical code, which could be expected since in the analytical model noise is not treated as precisely as in the numerical model. For example, speckles on sub-images are not taken into account, and noise propa-

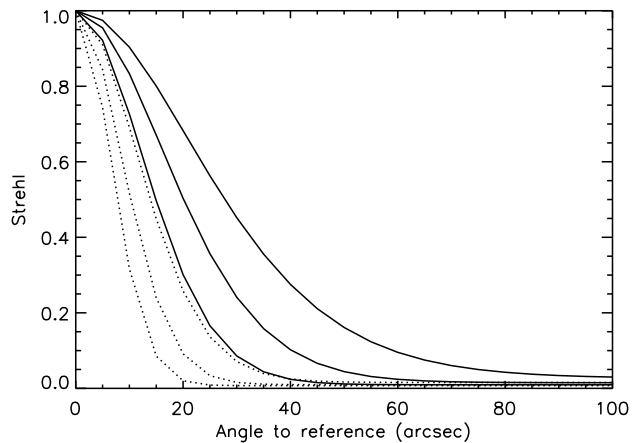


Figure 3. Anisoplanatism effect for an 8m telescope at $2.2 \mu\text{m}$ (K band), $1.65 \mu\text{m}$ (H band), $1.25 \mu\text{m}$ (J band), good model (solid) and median model (dots).

gation is less accurately modeled. The good agreement at the magnitude of the LGS allows us to use the analytical model. The behavior of the anisoplanatic effect was also validated with this model.

2.4 The LGS simulation

In the following, we assume that a sodium laser guide star, located at 90 km, is used. The laser power of 3-5 Watts creates a 10.5 magnitude guide star in the sodium layer. These values are representative of what has been achieved in experimentally (see e.g. (Jacobsen et al. 1994)).

Four effects specific to the LGS were simulated: cone effect, tilt anisoplanatism, error on the WFS due to the spot size and outer scale of turbulence (for the 8m case).

The cone effect was first pointed out by Foy & Labeyrie (1985) and has been studied by several authors (Fried (1994), Sasiela (1994), Tyler (1994)). The estimations given by these authors of the variance of the wavefront due to

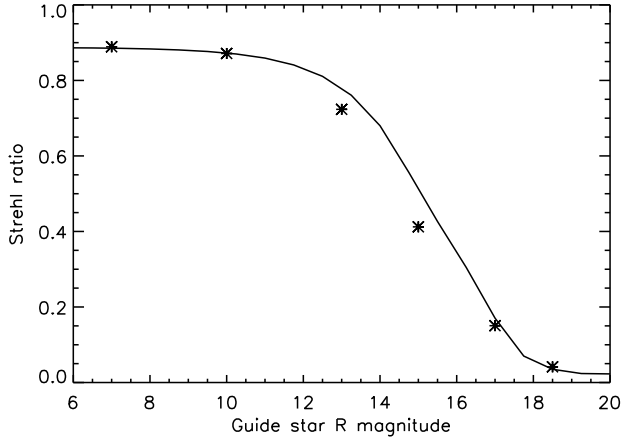


Figure 4. Comparison between the analytical AO model (solid) and the numerical model (stars) for 8m telescope at $2.2 \mu\text{m}$.

the cone effect are in good agreement. Therefore, the fastest method (Tyler (1994)) was used. The variance due to the cone effect is:

$$\sigma_{\text{cone}}^2 = \left(\frac{D}{d_0}\right)^{\frac{5}{3}} \quad (26)$$

$$d_0 = \lambda^{\frac{6}{5}} \cos^{\frac{3}{5}}(\zeta) \left[\int dh C_n^2(h) F\left(\frac{h}{H}\right) \right]^{-\frac{3}{5}} \quad (27)$$

where F is a numerical function and H is the laser star height.

Figure 5 represents the loss of Strehl only due to the cone effect. On a large telescope, the cone effect rapidly becomes the most important source of error. It reduces the maximum Strehl by a factor of 2 around $1.0 \mu\text{m}$ (depending on the C_n^2 profile). A loss of 80 percent occurs in the red, between 0.5 and $0.8 \mu\text{m}$. These curves underline the absolute necessity to find a solution to the cone effect, for example by considering a multiple LGS scheme (see e.g. Tallon & Foy (1990)).

When the science object is not bright enough for tilt sensing, one has to use a nearby tilt reference star. The variance caused by this effect, $\sigma_{\text{t-aniso}}^2$, was computed with eq.23. The corresponding loss of Strehl can be seen on Fig 6. A loss of 50 per cent occurs, in K (good model), at 75 arc-seconds. These results are in good agreement with Olivier & Gavel (1994) taking into account the differences in turbulence profiles, telescope diameters and hardware parameters.

The effect of the outer scale of turbulence on tilt anisoplanatism could be significative, if the outer scale, L_0 is comparable to the telescope diameter. L_0 is poorly known, the estimates range from a few meters to a few thousands of meters (see to summary of measurements in (Agabi et al. 1995)). However, recent measurements seem to converge to the same order of magnitude, from 20 to 50 meters. Therefore, we used the computations by Sasiela (1994) to get the effects of outer scale on tilt anisoplanatism, in the 8 meter case, assuming a Von Karman spectrum.

Three values for L_0 were used: 26m, 50m and infinite. Smaller values of L_0 were not considered because the expressions derived by Sasiela (1994) assume that $\pi D/L_0 < 1$. Fig 7 shows that the effect of the outer scale is not signif-

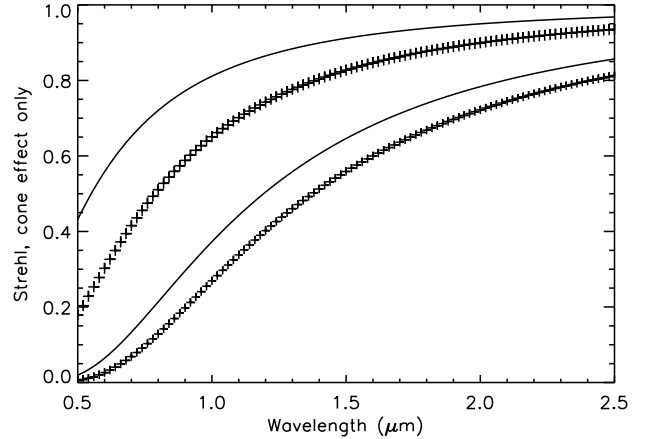


Figure 5. Wavelength dependence of cone effect for a 3.6m telescope (solid) and an 8m telescope (crosses). Good (above) and median (below) atmospheric models

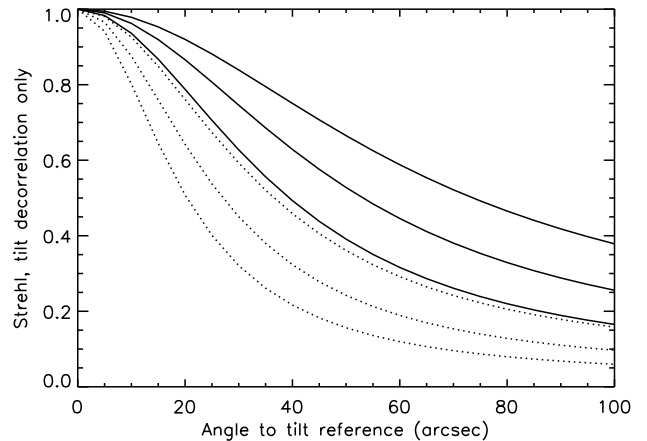


Figure 6. Tilt anisoplanatism: Wavelength and model comparisons for an 8m class telescope. Good (solid) and median atmosphere (dots), $\lambda = 2.2\mu\text{m}, 1.65\mu\text{m}, 1.25\mu\text{m}$ (top to bottom)

icant unless it is of the order of the size of the telescope (i.e the 26 meters case). Even in that case, the variation is smaller than the variation caused by seeing effects (at 100 arc-seconds, the difference in the extreme models is 30 per cent). Therefore, in the rest of this article, we assume an infinite outer scale.

When using a LGS, one has to be able to filter out the Rayleigh backscattering, created by the lower layers of the atmosphere, which can contribute to WFS noise if not filtered. The rejection can be done by emitting the laser through an off-axis beam projector and by spatially filtering the Rayleigh light with a field stop at the entrance focus of the WFS. In the following, the residual noise due to Rayleigh scattering was neglected.

The angle between the Rayleigh and the Sodium stars, θ , is given by a simple geometrical approach:

$$\theta = \frac{(H_{\text{Na}} - H_{\text{R}})d}{H_{\text{Na}}H_{\text{R}}} \quad (28)$$

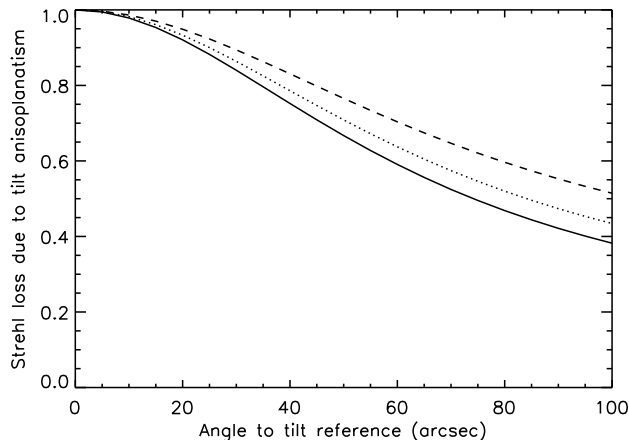


Figure 7. Outer scale of turbulence and tilt anisoplanatism: effects on an 8meter class telescope. $L_0 = \infty$ (solid), 50 m (dash), 26 m (dot). K band, good model.

where H_{Na} is the altitude of the Sodium layer (≈ 90 km), H_{R} is the altitude at the tip of the Rayleigh scattering region and d is the separation of the beam-projector and the considered sub-aperture. For an 8m telescope, assuming a distance of 1m between the beam projector and the primary mirror’s edge, the angular separation between the Rayleigh star’s tip and the sodium star varies from 8 arcsec to 72 arcsec, if the tip of the Rayleigh region is 20 km. However, the ATLAS experiment (Laurent (1996)) showed that at 20 km, one can still measure the Rayleigh backscattered flux. This is confirmed by LIDAR studies (see review by Gardner (1989)), showing that photocounts due to Rayleigh scattering reach the level of background noise near 50 km. If one considers that Rayleigh scattering stops at that height, the separation ranges then from 1.8 arcsec to 16.5 arcsec. This may be close enough to produce a measurable effect on the WFS and therefore reduce the quality of the correction. Another solution is to propagate the beam from the back of the secondary mirror. The separation of the two stars would be done with the help of the central obscuration (The Rayleigh scattering would be hidden by the secondary).

The elongation of the laser sodium spot, due to off-axis propagation, can be studied with a similar formula:

$$\theta_{\text{spot}} \sim \frac{\Delta H d}{H^2} \quad (29)$$

where ΔH is the thickness of the sodium layer (10 km). We obtain an elongation ranging from 0.25 arcsec to 2.3 arcsec.

The spot size can also be enlarged by the limitations of the optics and the laser itself. Therefore, we assumed that the spot size is independent of the seeing and fixed its value to 1.5 arcsec, with the elongation of the spot and with measured values of spot size (see e.g. (Jacobsen et al. 1994)). The increased size reduces the signal to noise ratio on the WFS. We neglected the effect of varying spot size on the pupil and took the mean value of elongation (center of the pupil to propagator). An effective r_0 was computed, giving the desired spot size. This mean size was injected in the noise calculations of the WFS (in eq. 14 and eq. 16). The effects of this spot size are small in K band (5 per cent max-

imum Strehl reduction), but become noticeable at shorter wavelengths (30 per cent in the I band).

Measurements of the height, density and thickness of the sodium layer ((Papen et al. 1996)) show significant variations in these quantities over periods of minutes. These variations can change the LGS brightness, and the variation of the focus. Therefore, sensing of the focus from another source than the LGS should be further investigated.

3 RESULTS

3.1 Estimated system performance

The final result for the Laser guide star system is obtained by adding the LGS-specific variances, neglecting possible correlations:

$$\sigma_{\text{tilt-LGS}}^2 = \sigma_{\text{tilt}}^2 + \sigma_{\text{t-aniso}}^2 \quad (30)$$

$$\sigma_{\text{ho-LGS}}^2 = \sigma_{\text{ho}}^2 + \sigma_{\text{cone}}^2 \quad (31)$$

The results showing the performances of a laser guide star system are presented on Fig 8 where it was assumed that the tilt reference is on-axis (i.e. the science object is bright enough for tilt sensing). Comparing the Strehl vs magnitude plots obtained in Fig. 2 and Fig. 8, we can see that the laser star has two main effects. It lowers the maximum Strehl that can be achieved with the AO system and drops, for the 8m system, from 0.87 to 0.75 in K for the good atmosphere (14 per cent reduction). At shorter wavelengths and median atmosphere model, the Strehl reduction is more severe (60 per cent in J for the median model). The effect is less severe on a 3.6m telescope (maximum loss: 60 per cent, the difference between the two La Silla seeing models being larger, as shown by Fig. 5). The second effect is that the limiting magnitude is much fainter with an LGS system. The 8m LGS-based system reaches a Strehl of 0.2 (K, good model) down to magnitude 19.5, which is 3.5 magnitudes fainter than with a NGS. A comparable gain is achieved on the 3.6m.

The cone effect is heavily C_n^2 dependent. In good conditions, one can achieve approximately the same Strehl in H band that can be achieved in K band when the atmosphere is median. In order to be able to use the LGS when it brings the best improvement, the location of the dominant turbulence layers should be known. If the turbulence is very high and the seeing is poor, the efficiency of the LGS will be severely affected (more than with conventional AO). This is especially true for the 8-m case, for which the cone effect is the dominant source of error. Therefore a device measuring the turbulence profile in real time, for example a SCIDAR (Azouit & Vernin (1980)) or a more simple device such as a measurement of the isoplanatic angle (Krause-Polstorff et al. 1993), even with a low accuracy, would help predicting what kind of performances can be expected from the LGS. This demonstrates the importance of queue scheduling, which sets observing priorities according to the atmospheric conditions: high angular resolution programs should have a high priority when the seeing-conditions are good.

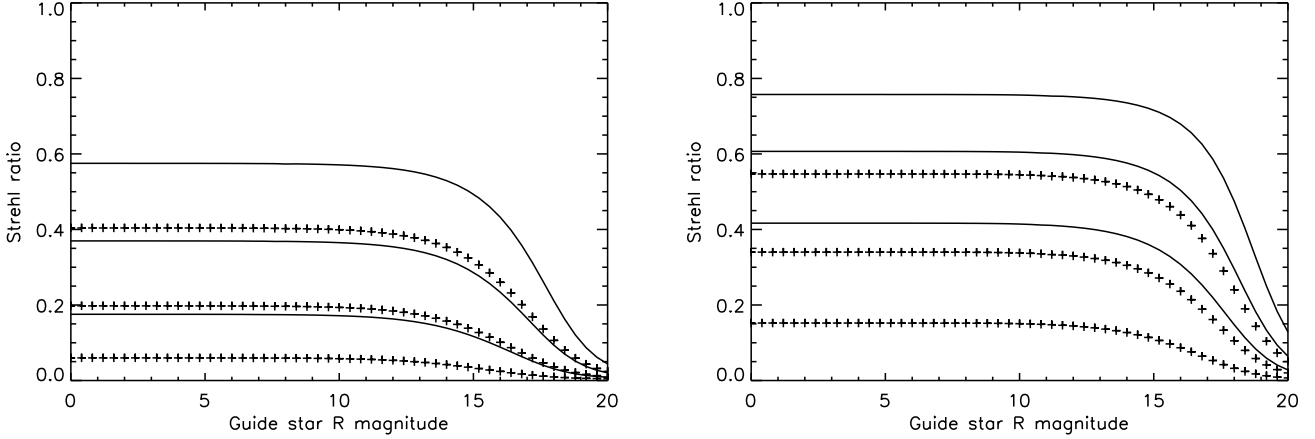


Figure 8. Performances for the AO+LGS systems (left: 3.6m, right: 8m), good (solid) and median (crosses) atmospheric model, in K, H, J bands (top to bottom). The reference star is on-axis.

3.2 FWHM estimation from Strehl

Usually, astronomers prefer to use FWHM of the PSF as an indicator of image quality rather than Strehl. In order to convert one to the other, we plotted the FWHM as a function of Strehl for the 3.6m and the 8m (Fig. 9). These figures were done using the good atmospheric model, varying the magnitude of the natural reference star. For a given Strehl, the LGS system has a wider PSF than the NGS system. For LGS systems, the short-exposure PSF is nearly diffraction limited, because the high orders are well corrected by the LGS. The long exposure Strehl degradation is due to the jitter caused by tilt measurement error (due to the faint magnitude of the tilt reference star and / or by tilt anisoplanatism), which moves this coherent peak. However, the energy stays in the coherent peak, which is wider because of the jitter, but does not contribute to the halo, like it does in a NGS system. This should be an advantage for example in the detection of faint companions. On NGS systems, the telescope diffraction limit can be achieved for Strehls of 0.1 - 0.2. Below these values, the coherent peak still exists but it is more difficult to extract information in these low corrections regimes. The limit-Strehl below which astronomical results cannot be obtained deserves further investigations.

3.3 Sky coverage

Two different methods were used to study the sky coverage. The first approach is statistical. The second one is a cross correlation of catalogues.

3.3.1 Statistical approach

To compute the statistical sky coverage, we used the so-called “Besançon model” (Robin & Cr ez e (1986)), which is a synthetic model of the Galaxy. At a given galactic latitude and longitude, it provides the density of stars that can be observed in a wavelength band.

Assuming that the position of the stars follow Poisson statistics, one can compute the probability P to find at least one star within a given radius r :

$$P_{N_{\text{stars}} > 0}(m, r) = 1 - e^{-\frac{\pi r^2 \eta(m)}{3600^2}} \quad (32)$$

where $\eta(m)$ is the density of stars brighter than magnitude m (per square degree) in the considered region (Besançon model).

For the galactic latitudes and longitudes we considered, we computed their most favorable zenith angles. An iso-Strehl plot was made at each of these angles. These plots were then overlaid on the iso-probability curves (Fig 10). It allowed us to get the statistical sky coverage values. For the 3.6m case, a K-Strehl of 0.2 can be achieved with a probability between 50 and 99 percent. A finer plot shows the probability to be 75 per cent.

The results obtained for the 3.6 m telescope and for the 8m in the K band can be found respectively on Tab. 3 and Tab. 5. Results for J band are presented in Tab. 4 (3.6m telescope) and Tab. 6 (8m case). The first percentage represents the probability (in per cent) for a given Strehl for the good seeing atmospheric model. The second number is for the median atmospheric model. The Strehl differences between the galactic pole and the galactic center can easily be explained. There is a higher stellar density near the center, which allows to find a closer reference star. However, there is a second effect that reduces even more the Strehl at the pole. Indeed, at Paranal and La Silla, the galactic center is almost at 0 zenith angle. On the other hand, the galactic pole region is fairly low in the sky. This effect reduces even more the sky coverage obtained.

In K band, the LGS brings a significant improvement of the sky coverage in all cases, whether the atmospheric conditions are good or median and at all stellar densities. A 30 per cent sky coverage (at 0.5 Strehl) is achieved with average stellar densities, when a coverage of only 2 per cent was possible with NGS, under good seeing conditions (8m case). Note that the sky coverage can drop from 80 per cent to 15 per cent on a NGS system simply because the atmospheric conditions change. For the 3.6 meter case, the gain goes from a factor of 2 (low Strehl, high star count, K band), to a factor of 100 at low Strehls and low star counts.

For J band, the conclusion is less obvious. Sky coverage is low (except near the pole, where it can be good at

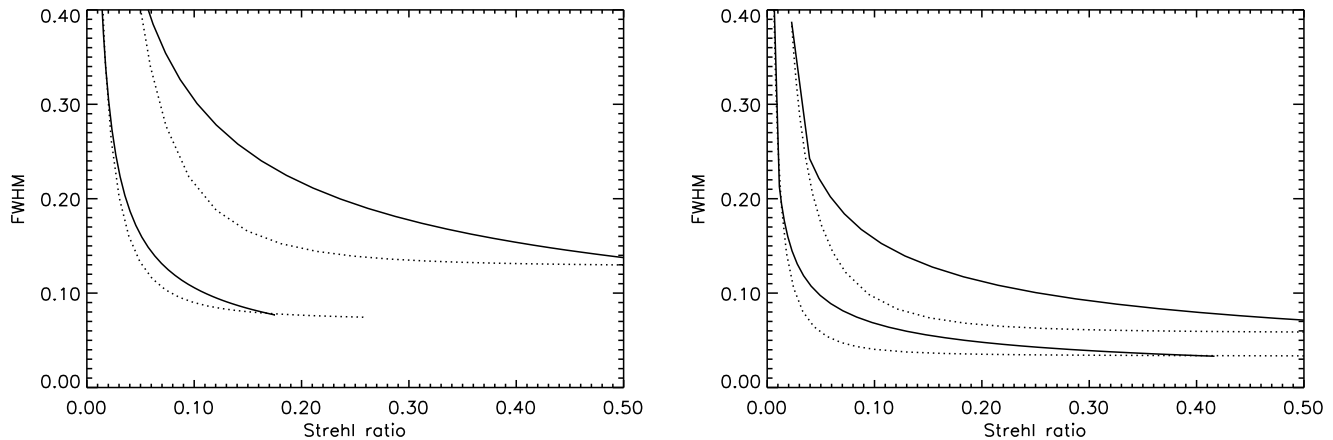


Figure 9. FWHM (arcsec) vs Strehl at $2.2 \mu\text{m}$ (top) and $1.25 \mu\text{m}$ (bottom) for the 3.6 m case (left) and the 8 m case (right), good model. NGS AO (dotted) and LGS AO (solid).

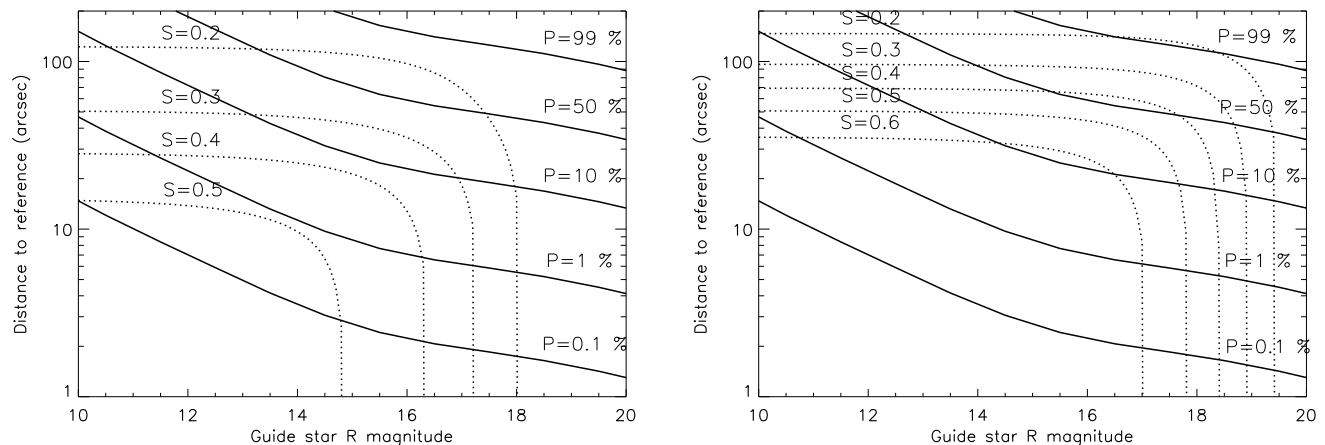


Figure 10. Iso-Strehl curves (dotted) for 3.6m + LGS(left) and 8m + LGS (right). Probability to find a reference star (solid) at galactic longitude (l) = 180, latitude (b) = 20. Notice logarithmic scale for distances.

Table 3. statistical sky coverage - 3.6m case, K band

K Strehl	Center	Average ¹	Pole
$S_{\text{NGS}} = 0.2$	20 - 1	1 - 0.08	0.01 - <0.01
$S_{\text{LGS}} = 0.2$	99 - 70	75 - 5	0.5 - <0.01
$S_{\text{NGS}} = 0.3$	8 - 0.3	0.6 - 0.05	<0.01
$S_{\text{LGS}} = 0.3$	99 - 10	25 - 0.5	0.08 - <0.01

¹: $l=180, b=20$.

low Strehls), and sometimes NGS gives better performances than LGS (8m case, median seeing, Strehls of 0.2 and 0.3). However, in good seeing cases, the LGS still gives better results than NGS (factor of 30 better for $S=0.2$ at average densities). It can go from a factor of 3 (Strehl of 0.2) to more than a factor 100 (near the pole). The sensitivity to seeing conditions is also greater than in K band (because of the cone effect which is wavelength dependent). There-

Table 4. statistical sky coverage - 3.6m case, J band

J Strehl	Center	Average ¹	Pole
$S_{\text{NGS}} = 0.1$	0.8 - <0.01	0.6 - <0.01	<0.01
$S_{\text{LGS}} = 0.1$	40 - <0.01	3 - <0.01	<0.01

¹: $l=180, b=20$.

fore, in J band, to get a gain with the LGS, favorable seeing conditions are needed.

3.3.2 Catalogue cross correlations

The second approach to study sky coverage is to make cross correlations of catalogues. We selected several categories of astronomical objects, in two categories: extragalactic and stellar.

In the extragalactic domain, the Veron-Cetty 96 (Veron-

Table 5. statistical sky coverage - 8 m case, K band

K Strehl	Center	Average ¹	Pole
$S_{NGS} = 0.2$	80 - 15	10 - 1	0.5 - 0.05
$S_{LGS} = 0.2$	99 - 99	99 - 33	10 - 0.8
$S_{NGS} = 0.3$	60 - 8	8 - 0.7	0.2 - 0.02
$S_{LGS} = 0.3$	99 - 99	75 - 12	5 - 0.08
$S_{NGS} = 0.5$	20 - 1	2 - 0.1	0.07 - < 0.01
$S_{LGS} = 0.5$	99 - 8	30 - 0.5	0.7 - < 0.01

¹: l=180, b=20.

Table 6. statistical sky coverage - 8 m case, J band

J Strehl	Center	Average ¹	Pole
$S_{NGS} = 0.1$	30 - 2	2 - 0.2	0.07 - < 0.01
$S_{LGS} = 0.1$	99 - 20	70 - 1	1 - < 0.01
$S_{NGS} = 0.2$	10 - 0.5	0.8 - 0.07	0.03 - < 0.01
$S_{LGS} = 0.2$	99 - < 0.01	25 - < 0.01	0.08 - < 0.01
$S_{NGS} = 0.3$	5 - 0.08	0.5 - 0.02	< 0.01
$S_{LGS} = 0.3$	70 - < 0.01	6 - < 0.01	< 0.01

¹: l=180, b=20.

Cetty & Veron (1996)) catalogue was used. This catalogue contains 8609 Quasars and 2833 Active Galactic Nuclei (AGN). In the stellar domain, the SIMBAD database was used. Several types of stars were studied: Miras (total number of objects: 4279), Semi Regular pulsating variables (SRs, 2182 objects), and Pre-Main Sequence stars (PMS, 928 objects). We used the US Naval Observatory A-V1.0 catalogue (USNOC) to search for reference stars around these objects.

Because the chosen stellar objects are variable and the amplitude of their variations is not always well known, an approximation was used: in order to get the brightness of the minimum, 4 magnitudes were added to the magnitude of the bright phase, found in the catalogue (except for SRs, 2 magnitudes). For Miras, for example, the variability ranges from 2.5 to 6 mag in V band (Van Belle et al. 1996), so 4 magnitudes can be seen as an “average” variability. Therefore, each variable star has two magnitudes: the bright and the faint phase.

Another magnitude correction was applied. Usually, the SIMBAD catalogue contain only V-band magnitudes. However, the WFS is used in the red part of the spectrum (near the R band). We took, as a first order approximation, average V-R correction terms. Using the General Catalogue of Variable Stars (GCVS, (Kholopov et al. 1985-1988)), the mean spectral type of M-type Miras (the most numerous) was computed. A sample of 400 Miras was used. The mean spectral type is M4.4 at maximum and M7.1 at minimum. The corresponding V-R indexes are 1.7 and 2.2 respectively. The same procedure was applied to SRs. We used a sample of 107 objects, the spectral type varies from M4.5 (V-R=1.7) to M6.5 (V-R=1.9). The variation is smaller than for the Miras, which was expected. For the PMS objects, we used the mean of a sample of 76 T-Tauri star V-R measurements, taken from (Herbst, Herbst & Grossman 1994). This leads to a V-R index of 0.79. Because the spectra of Quasars and AGN is very object-dependent, we did not apply any correc-

tion. A slight bias for these objects is therefore not excluded. We did not apply any magnitude correction to the USNOC reference stars, because it contains R-band magnitudes.

One problem in the correlation approach is not to count an object twice. Indeed, because of the imprecision in the coordinates of an object, one can select it as a science object, and find it also in the USNOC and count it as its own reference. This would overestimate the number of objects that can be observed. It was decided not to select references closer than 3 arc-seconds to the object. We do not exclude that despite this procedure, some objects have been counted twice.

For computational reasons, a radius limited to 240 arc-sec was searched around the object to find a reference. The number of references was limited to the 20 closest. When a reference was found, the Strehl was computed, taking into account the following factors: distance and magnitude of the reference, brightness of the laser star, zenith angle at Paranal (La Silla). The procedure was applied to NGS and LGS AO, for good and median atmospheric conditions. When several references were found for an object, the one providing the best Strehl was selected. Strehl ratios were also computed for all the science objects on-axis, assuming that the reference was a point source of the magnitude stated in the catalogue (which can be a crude approximation for AGN for example, which are extended objects, and leads a over-estimation of the Strehl for these objects). This procedure was applied in J and K bands. The results for the 3.6m are in Tab. 7 and Tab. 8, and those for the 8m are in Tab. 9 and Tab. 10. We have included in these tables $\langle S_{NGS} \rangle$ ($\langle S_{LGS} \rangle$) the mean Strehl, in per cent, with NGS (LGS) on each class of objects (for variable stars, the first number indicates maximum brightness, the second the minimum brightness), $\sigma_{S_{NGS}}$ ($\sigma_{S_{LGS}}$) the standard deviation on this Strehl, and $N_{S>0.1}$ and $N_{S>0.2}$, the number of objects than can be observed with a Strehl greater than 0.1 or 0.2.

Several comments can be made about these numbers. The first is that the improvement due to the laser star in K band is obvious: for faint objects, the Strehl ratio and the number of observable object are notably increased. The gain of the LGS is maximum for faint objects (like quasars, mean magnitude: 18.2, AGN: 16.7), for which the gain in Strehl can be as high as a factor of 10 (8m case). Bright objects (SRs, at maximum (mean magnitude of 12.3), Miras at maximum, (mean magnitude: 12.6)) can be used as reference for the NGS system, which gives high Strehls (no cone effect), and therefore benefit less from the laser star. The number of objects is also increased considerably with the LGS: for the 8m, the number of quasars goes from hundreds (21-357) to thousands (2893-6803). Another important factor is the influence of seeing conditions. The fainter the objects, the more it affects AO performance: for the 3.6m, the number of quasars observable with the LGS can range from 287 to 3809. This is due to the sensitivity of the LGS to high altitude turbulence and because for these objects, the limiting magnitude of the system is close to the magnitude of the objects (see Fig. 8). On NGS AO, the differences are not as important (which confirms the dominant effect of the cone effect). This emphasizes again the need to be able to estimate the high altitude turbulence component.

Like in the statistical approach, the results in J are more contrasted. One can get a tremendous improvement on faint

Table 7. 3.6m - astrophysical targets, K band. GS: Good seeing, MS: Median seeing. Strehls are in per cent.

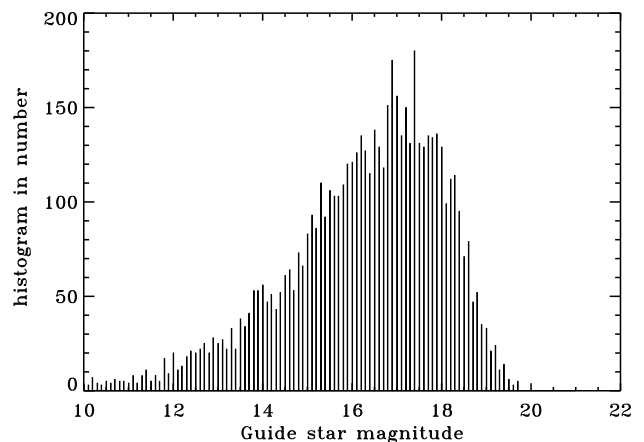
Object	$\langle S_{NGS} \rangle$	$\sigma_{S_{NGS}}$	$N_{S>0.1}$	$N_{S>0.2}$	$\langle S_{LGS} \rangle$	$\sigma_{S_{LGS}}$	$N_{S>0.1}$	$N_{S>0.2}$
Quasar - GS	2.5	2.2	115	23	18.6	10.6	6352	3809
Quasar - MS	1.4	0.6	4	0	7.2	5.4	1890	287
AGN - GS	6.6	11.9	426	273	23.9	16.9	1931	1517
AGN - MS	3.0	6.3	206	106	12.0	11.1	1198	671
PMS - GS	19.7 - 7.5	17.4 - 10.6	542 - 185	377 - 118	40.6 - 28.3	12.0 - 13.5	900 - 835	846 - 671
PMS - MS	10.7 - 2.8	13.0 - 5.1	319 - 61	195 - 21	23.7 - 13.2	9.59 - 8.8	810 - 521	680 - 216
SR - GS	29.6 - 21.4	19.2 - 19.2	1686 - 1295	1420 - 941	35.6 - 34.2	16.1 - 15.7	1885 - 1891	1754 - 1724
SR - MS	19.1 - 12.3	16.0 - 15.2	1339 - 780	904 - 546	20.5 - 19.0	11.7 - 11.2	1649 - 1594	1232 - 1086
Miras - GS	30.8 - 13.6	18.4 - 16.2	3526 - 1697	2944 - 1115	35.8 - 31.0	16.1 - 15.5	3765 - 3686	3512 - 3171
Miras - MS	19.8 - 6.5	15.4 - 11.1	2795 - 826	1934 - 518	20.6 - 16.2	11.8 - 10.7	3313 - 2853	2364 - 1597

Table 8. 3.6m - astrophysical targets, J band. GS: Good seeing, MS: Median seeing. Strehls are in per cent.

Object	$\langle S_{NGS} \rangle$	$\sigma_{S_{NGS}}$	$N_{S>0.1}$	$N_{S>0.2}$	$\langle S_{LGS} \rangle$	$\sigma_{S_{LGS}}$	$N_{S>0.1}$	$N_{S>0.2}$
Quasar - GS	0.5	0.2	0	0	2.6	2.0	60	0
Quasar - MS	0.3	0.1	0	0	0.6	0.4	0	0
AGN - GS	1.1	2.7	74	5	4.2	4.3	359	0
AGN - MS	0.4	0.7	1	0	1.1	1.2	0	0
PMS - GS	3.0 - 0.9	4.5 - 1.7	91 - 9	8 - 0	8.0 - 4.5	3.9 - 3.2	309 - 73	0 - 0
PMS - MS	1.1 - 0.4	2.1 - 0.5	12 - 0	0 - 0	2.0 - 1.0	1.2 - 0.8	0 - 0	0 - 0
SR - GS	5.5 - 3.7	6.5 - 5.8	471 - 302	101 - 55	6.4 - 6.0	4.9 - 4.6	570 - 454	0 - 0
SR - MS	2.3 - 1.5	3.4 - 2.8	116 - 74	0 - 0	1.6 - 1.4	1.5 - 1.4	0 - 0	0 - 0
Miras - GS	5.6 - 2.0	6.2 - 3.8	930 - 267	166 - 22	6.5 - 5.0	5.0 - 4.3	1239 - 647	0 - 0
Miras - MS	2.2 - 0.7	3.2 - 1.6	189 - 22	0 - 0	1.6 - 1.2	1.6 - 1.2	0 - 0	0 - 0

objects compared to NGS (e.g. from 12 to 1119 quasars on the 8m). In almost all cases, when the seeing is good, the LGS improves the situation, although sometimes marginally (like for the SRs). If the seeing is median, faint objects (like quasars, AGN) are difficult to observe with good performances (with $S > 0.2$, no quasars, only 68 AGN for 8m NGS, and none with the LGS). It is not unusual that better results are obtained with NGS for median seeing, which is the same conclusion as with statistical methods, although some exceptions are present (8m, quasars and AGN with $S > 0.1$). It appears that most of the time, the best Strehl is achieved on-axis, even if a reference star is found, and can be seen by the change in Strehl when going from bright to faint phase of variable stars. Indeed, if external references were used in a majority of cases, the brightness of the central object would not matter. The reason for this behavior can be explained by several arguments. First, when looking at Fig 8, we can see that the LGS is at maximum Strehl down to magnitude 15-16 (8m case), so an external reference is not needed at these magnitudes. A second reason is that since science catalogues are incomplete, bright objects will dominate the catalogue, and they can be observed on-axis. A third reason is that for two nearly equivalent brightness objects, the on-axis one will give better performances, because there is no anisoplanatism.

A second point is the incompleteness of the USNOC. The number of bright stars will be over-estimated compared to fainter ones, and therefore the references will be statistically further away from the science object, yielding to an under-estimation of Strehl. It also means that the numbers


Figure 11. Histogram of the magnitude of the stars found in the USNOC, yielding the best Strehl when used as a reference

we have derived are lower limits, since all the stars suitable as references are not in the catalogue. On Fig. 11, we plotted the magnitudes of the reference stars giving the best Strehl ratio. It can be seen that stars close to magnitude 20 were found in this catalogue, which is a considerable improvement to the Hubble Space Telescope Guide Star Catalogue (complete to about magnitude 14.5, (Jenkner et al. 1990)) which was used in an earlier version of this study. This histogram is a convolution of two effects: the magnitude dependance of

Table 9. 8m - astrophysical targets, K band. GS: Good seeing, MS: Median seeing. Strehls are in per cent.

Object	$\langle S_{NGS} \rangle$	$\sigma_{S_{NGS}}$	$N_{S>0.1}$	$N_{S>0.2}$	$\langle S_{LGS} \rangle$	$\sigma_{S_{LGS}}$	$N_{S>0.1}$	$N_{S>0.2}$
Quasar - GS	4.4	7.2	819	357	37.2	17.0	7651	6803
Quasar - MS	1.2	2.0	63	21	16.7	10.6	5953	2893
AGN - GS	15.4	23.1	895	698	43.0	23.3	2329	2077
AGN - MS	6.9	15.2	426	315	22.6	17.0	1850	1393
PMS - GS	45.2 - 19.8	27.1 - 23.1	771 - 439	710 - 317	63.0 - 50.0	14.0 - 19.2	918 - 868	892 - 822
PMS - MS	25.4 - 7.6	23.7 - 14.2	568 - 180	443 - 127	38.9 - 26.5	12.4 - 14.0	870 - 777	842 - 624
SR - GS	61.4 - 49.5	23.0 - 26.6	2020 - 1896	1961 - 1768	57.8 - 56.9	18.3 - 18.0	2050 - 2055	1984 - 1990
SR - MS	42.2 - 29.4	23.9 - 25.5	1835 - 1426	1663 - 1159	33.8 - 32.6	15.5 - 15.1	1877 - 1884	1721 - 1696
Miras - GS	63.5 - 35.4	21.3 - 27.2	4084 - 3189	3961 - 2660	57.9 - 54.1	18.1 - 18.4	4096 - 4041	3960 - 3906
Miras - MS	44.2 - 17.4	22.4 - 22.0	3772 - 1811	3530 - 1342	33.8 - 29.7	15.4 - 14.9	3748 - 3679	3450 - 3148

Table 10. 8m - astrophysical targets, J band. GS: Good seeing, MS: Median seeing. Strehls are in per-cent.

Object	$\langle S_{NGS} \rangle$	$\sigma_{S_{NGS}}$	$N_{S>0.1}$	$N_{S>0.2}$	$\langle S_{LGS} \rangle$	$\sigma_{S_{LGS}}$	$N_{S>0.1}$	$N_{S>0.2}$
Quasar - GS	0.7	1.5	43	12	11.0	7.6	4214	1119
Quasar - MS	0.2	0.2	1	0	2.1	1.9	40	0
AGN - GS	4.9	12.2	350	241	15.4	12.5	1568	965
AGN - MS	1.6	5.3	148	68	3.6	3.9	287	0
PMS - GS	17.9 - 5.4	18.7 - 10.9	476 - 147	346 - 104	27.3 - 18.2	9.5 - 10.2	854 - 702	760 - 422
PMS - MS	6.5 - 1.3	10.6 - 3.9	203 - 35	124 - 14	7.1 - 3.9	3.5 - 2.99	196 - 46	0 - 0
SR - GS	30.4 - 21.1	20.2 - 20.6	1670 - 1213	1411 - 898	22.9 - 22.1	12.1 - 11.7	1736 - 1727	1406 - 1360
SR - MS	13.7 - 8.7	13.9 - 12.9	1017 - 619	632 - 418	5.5 - 5.2	4.3 - 4.0	387 - 296	0 - 0
Miras - GS	31.7 - 12.4	19.2 - 0.17	3516 - 1497	2975 - 1045	23.0 - 19.8	12.2 - 11.5	3481 - 3231	2701 - 2271
Miras - MS	14.1 - 4.2	13.3 - 9.0	2156 - 616	1294 - 371	5.6 - 4.4	4.4 - 3.8	868 - 428	0 - 0

the AO system (faint sources are not selected as references), and the magnitude distribution of the catalogue. The peak of Fig. 11 is near magnitude 17, whereas the peak distribution of star for the USNOG is near 19. Therefore, this study should suffer less from incompleteness than when using the GSC.

The LGS can significantly increase the number of objects that can be observed in each class, so that statistical studies on these objects can be performed. The performances that can be expected on individual objects are also very promising. On each class of objects, one can find targets that allow high performance observations. Indeed, there are objects with high Strehl ratios and that could not be observed with the AO system without the LGS. In J band, the LGS improves the performances of the system, but only when the atmospheric conditions are good. The number of objects that can be observed with good performances is drastically reduced, but in good seeing, there is still a large sample of objects (e.g. 1119 quasars, 965 AGN with $S > 0.2$) to make statistical studies. With NGS, this is not as obvious (only 8 quasars, 128 AGN for the same conditions). However, even if the Strehl is lower, and therefore the gain in signal to noise ratio obtained by the correction is smaller, the diffraction limit in J is also smaller, so one can have a better resolution. Thus the LGS can be used in J band, under good seeing conditions, to improve the performances of the AO system.

4 LGS IN THE VISIBLE

To see the possibilities of the laser star in the visible part of the spectrum, we chose an excellent atmospheric model. This model uses a seeing of 0.3 arcsec, which can be obtained approximately 10 per cent of the time, turbulence heights and wind profile being the same as in the good seeing model previously used. The isoplanatic angle was chosen to be larger than in the good model, 6.0 arcsec (at 0.5 μm). This was done by modifying the strength of the layers. Fig. 12 represents the Strehl with and without a LGS, on the 8m system, as a function of the on-axis reference star R magnitude. The solid curves are for the LGS AO, in excellent and good seeing conditions. The dotted curves represent NGS AO for the same seeing conditions. It can clearly be seen that when the atmospheric conditions are excellent, but not unrealistic, a reasonable Strehl can be achieved with the laser star in the red. At H_α (0.656 μm), a Strehl of 0.2 can be achieved with the LGS down to magnitude 13-15, which is a significant improvement. The dotted curve represents the performances of NGS AO, in the same conditions. Because there is no cone effect, the Strehl ratio can be as high as 0.55 at H_α , in exceptional seeing. At that wavelength, the diffraction limit of an 8m telescope is 17 milli-arcseconds, which can be achieved with both methods. This is nearly 4 times better than the diffraction limit of the HST. The gain obtained with astronomical NGS AO in the red has already been experimentally confirmed, on the CFHT AO bonnette, PUEO (Rigaut et al. 1997b).

This result clearly shows that adaptive optics and LGS

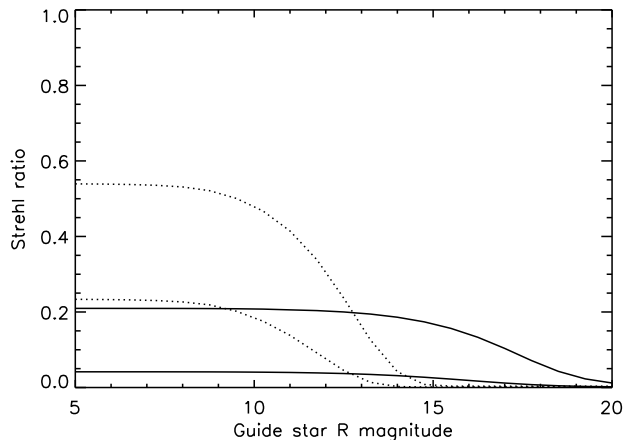


Figure 12. Strehl NGS (dots), LGS (solid), for excellent (NGS, LGS), and good seeing conditions, at H_{α} .

adaptive optics are not limited to the infrared part of the spectrum as it is often thought.

5 CONCLUSIONS

The necessity of having favorable atmospheric conditions to get good performances with AO in general and LGS AO in particular underlines the need for flexible scheduling. One has to be able to program high angular resolution observations when the seeing is good. A mean of measuring, even crudely, the C_n^2 profile on-line would be of crucial importance to be able to predict if LGS observations are feasible, because of the height dependence of the cone effect. A SCIDAR or a more simple device, giving measurements of the high altitude component of turbulence, would therefore be of prime importance.

We have shown shown that good performances can be achieved in the visible, when atmospheric conditions are good (1 night over 10) with adaptive optics. It is reminded that astronomical adaptive optics is not limited to the near infra-red domain, as it is often thought in the astronomical community.

The problem of knowing what Strehl ratio yields acceptable astrophysical results should be studied in more detail. We chose to take two cases, 0.1 and 0.2. However, it seems likely that with proper deconvolution methods, reliable astrophysical results can be obtained with lower Strehls. The limit is probably not sharp and depends on the class of object being observed, but deserves further investigation. The different behavior of the point spread function between NGS and LGS and its astrophysical implications should also be studied.

This study has shown the imperative need, for 8m class telescopes to find a solution for the cone effect. Indeed, as shown by both sky coverage approaches, a good Strehl ratio can be achieved on a large amount of astrophysical objects in the red, with the laser guide star, only with good (or excellent) seeing, because of the cone effect.

The tilt determination problem is also important. As shown by the statistical approach, a full sky coverage cannot

be achieved with the LGS. Galactic poles cannot be fully exploited at high angular resolution, because of the lack of nearby tilt-reference stars. To achieve full coverage, the only solution is to get tilt information from the laser star (either the polychromatic method or a combination of the laser-strip observing methods).

However, we have shown in this study, by two different methods, that the simplest Laser Guide Star, without correction of the cone effect and using a natural star for tilt determination, can bring a significant improvement in sky coverage in the K band, both on 3.6m and 8m telescopes. We made approximations to correct for the V-R values for the observed objects, since the wavefront sensing is done in the red. For an atmospheric model representing the best 20 per cent of the time, the sky coverage is nearly complete in the galactic plane for Strehls of 0.3 (for the 3.6m) or 0.5 (for the 8m). At average galactic latitudes, the coverage drops to 25 per cent (3.6m) and 30 per cent (8m). Near the pole, the figures become small (0.08 and 0.7), because tilt-reference stars are not found close to the science object. We have also shown that the sky coverage and the improvement due to the LGS are very sensitive to seeing conditions. For atmospheric models representing median values, the sky coverage values drop to 10 per cent (3.6m) and 8 per cent (8m) for 0.3 and 0.5 Strehl. The improvement in terms of observable objects is also important. The number of observable quasars with Strehl greater than 0.2 is increased from 23 to 3809 for the 3.6m and from 357 to 6803 on the 8m (good seeing). For stellar objects, whose population is dominated, in the catalogues, by bright objects do not benefit as much from the LGS, since for example, the semi-regular pulsating variables, for which the average magnitude is as bright as 12.3 at maximum, are better observed with the Natural guide star. However, in a vast majority of cases, the LGS gives much better performances than NGS in the K band, the biggest increases being for the faintest objects. In J band, the improvement is smaller and very much seeing dependent. In good seeing, the LGS still improves the performances of the system (e.g. it brings 60 quasars in the 3.6m case, where none were accessible with NGS; for the 8m, the number of AGN with Strehls greater than 0.2 goes from 241 to 965). However, in median seeing, it can be preferable to use the NGS system, because the cone effect reduces very much the performances of the system (for example, 124 pre-main sequence stars can be observed at 0.2 Strehl with the 8m-NGS, and none with the LGS).

ACKNOWLEDGEMENTS

The authors would like to thank A. Robin, from Observatoire de Besançon for providing the stellar population models, F. Rigaut for providing us the AO simulation code and for fruitful discussions, D. Bonaccini for his help on AO simulations, M. Sarazin for insightful discussions on atmospheric models, and Eric Thiébaud for his help. This research has made use of the SIMBAD database, operated at CDS, Strasbourg, France, and of the USNO-A-V1.0 catalogue. This work has benefitted from discussions during meetings of the Laser Guide Star TMR network of the European Union, contract #ERBFMRXCT960094.

REFERENCES

- Agabi A., Borgnino J., Martin F., Tokovinin A., Ziad A., 1995, *A&ASS*, 109, 557
- Azouit M., Vernin J., 1980, *J. Atmos. Sci.*, 37, 1550
- Babcock H. W., 1953, *PASP*, 65, 229
- Beuzit J.-L., et al., 1994, *SPIE* 2201
- Bonaccini D., 1996, ESO technical report, VLT-TRE-ESO-11630-1137
- Chassat F., 1989, *J. Optics*, 20
- Foy R., Labeyrie A., 1985, *A&A*, 152, L29
- Foy R., Migus A., Biraben F., Grynberg G., McCullough P.R., Tallon M., 1995, *A&ASS*, 111, 569
- Fried D. L., 1966, *J. Opt. Soc. Am.*, 56, 10
- Fried D. L., 1982, *J. Opt. Soc. Am. A*, 1, 72
- Fried D. L., Belscher J. F., 1994, *J. Opt. Soc. Am. A*, 11, 1
- Friedman H., Foy R., Tallon M., Migus A., 1996, *Proc. OSA topical meeting on adaptive optics*, Maui, in press
- Fuchs A., Vernin J., 1993, VLT technical report VLT-TRE-UNI-17400-0001
- Fugate R. Q., et al., 1994, *J. Opt. Soc. Am. A*, 11, 1
- Gardner C. S., 1989, *Proc. SPIE*, 77, 3
- Gilmore G., King I., Van der Kruit P., 1989, *The Milky Way as a galaxy*, Nineteenth advanced course, Swiss society of astrophysics and astronomy Saas-Fee
- Greenwood D.P., 1977, *J. Opt. Soc. Am.*, 67, 3
- Greenwood D.P., 1979, *J. Opt. Soc. Am.*, 69, 4
- Herbst W., Herbst D.K., Grossman E.J., 1994, *AJ*, 108, 5
- Jacobsen B., Martinez T., Angel R., Lloyd-Hart M., Benda S., Middleton D., Friedman H., Erbert G., 1994, *Proc SPIE*, 2201
- Jankevics A. J., Wirth A., 1991, *SPIE* 1543
- Jenkner H., Lasker B.M., Sturch C.R., Mclean B.J., Shara M.M., Russel J.L., 1990, *AJ*, 99, 2081
- Johnston D.C., Welsh B.M., 1994, *J. Opt. Soc. Am. A*, 11, 1
- Kholopov P.N., 1985-1988, *General Catalogue of Variable Stars*, 4th edition (Moscow: Nauka Publishing House)
- Krause-Polstorff J., Murphy E.A., Walters D.L., 1993, *Appl. Opt.*, 32, 4051-4057
- Lai O., 1996, these de l'universite Paris 7
- Laurent S., 1996, thèse de l'université Paris 6
- Laurent S., et al., 1995, *Proc. ESO/ESA conference on adaptive optics*, Garching
- Max C. E., et al., 1994, *J. Opt. Soc. Am. A*, 11, 2
- Olivier S., Gavel D., 1994, *J. Opt. Soc. Am. A*, 11, 368-378
- Papen G. C., Gardner C. S., Yu J., 1994, *OSA technical Digest on the Adaptive Optics conference (Maui)*, 13
- Parenti R., 1992, *Lincoln laboratory journal*, 5, 1, 93-114
- Parenti R., Sasiela R. J., 1994, *J. Opt. Soc. Am. A*, 11, 288-309
- Ragazzoni R., 1997, *A&A*, 319, L9
- Rigaut F., 1994, in D. M. Alloin and J. M. Mariotti, eds., *Adaptive optics for astronomy*, NATO ASI
- Rigaut F., 1996, in *High angular resolution in astrophysics*, NATO ASI, in press
- Rigaut F., Gendron E., 1992 *A & A*, 261, 677-684
- Rigaut F., Ellerbroek B.L., Northcott M., 1997, *Appl. Opt.*, 36, 13, 2856
- Rigaut F., et al., 1997, to be submitted
- Robin A., Crézé M., 1986, *A & A*, 157, 71-90
- Roddier, F., Gilli, J.M., Vernin, J., 1982, *J. Optics*, 13, 2
- Rousset G., in D. M. Alloin and J. M. Mariotti, eds., *Adaptive optics for astronomy*, NATO ASI
- Sarazin M., 1990, M. Sarazin ed., *VLT Report No 60*
- Sasiela R. J., 1994, *Electromagnetic wave propagation in turbulence*, L. M. Brekhovskikh, L. B. Felsen, H. A. Haus eds., Springer-Verlag
- Sandler D.G., Stahl S., Angel J.R.P., Lloyd-Hart M., McCarthy D., 1994, *J. Opt. Soc. Am. A*, 11, 2
- Tallon M., Foy R., 1990, *A&A*, 235, 549
- Tessier, E., 1997, *A&A*, in press
- Tyler G. A., 1994, *J. Opt. Soc. Am. A*, 11, 325-338
- Van Belle G.T., Dyck H.M., Benson J.A., Lacasse M.G., 1996, *AJ*, 112, 5
- Veron-Cetty M., Veron P., 1996, *A catalogue of quasars and active nuclei*, 7th edition, ESO Sci report, 17, 1-276

This paper has been produced using the Royal Astronomical Society/Blackwell Science L^AT_EX style file.